ACS Macro Letters

pubs.acs.org/macroletters Letter

Effects of Molecular Weight and Surface Interactions on Polymer Diffusion in Confinement

Brittany K. Roopnarine, Spencer C. Schmidt, Kevin J. Maxwell, and Svetlana Morozova*

Cite This: ACS Macro Lett. 2023, 12, 221−226 Read Online

ACCESS | Metrics & More | Article Recommendations | Supporting Information

ABSTRACT: Understanding the transport and thermodynamics of polymers in confined spaces is helpful for many separation processes like water purification, drug delivery, and oil recovery. Specifically, for water purification, dextran has been used as a "model" foulant. Uncovering how these polymers interact in confinement can reduce the fouling of organic membranes and will lead to better separation processes overall. We have determined the diffusion coefficient, D, of dextran and sodium polyacrylate in convex lens-induced confinement using differential dynamic microscopy. In this setup, the gap height ranges continuously from 0.077−21.8 μm. It was found that polymer diffusion becomes slower in higher confinement, which is consistent with a change in the increase of the hydrodynamic resistance to macromolecule motion and depends on the surface properties. These findings indicate that dextran diffusion changes in confinement and can lead to a better understanding of separation processes.

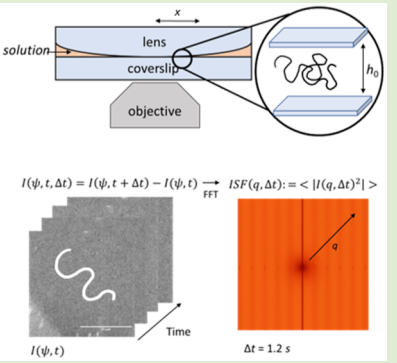

Polymer diffusion in confinement is important for many applications such as membrane separation,[1−4] oil recovery,[5,6] and materials processing.[7,8] In oil recovery, polyacrylamide and other polymers are used as additives to aid the process.[5,6] More specifically for membrane separation, polysaccharides like dextran typically foul poly(ether sulfone) (PES) ultrafiltration (UF) membranes.[9,10] Because of this it is important to understand how these model foulants diffuse in confinement, which can lead to more efficient membrane separation and aid separation processes overall. In this Letter we have determined the diffusion of dextran and sodium polyacrylate in confinement using Differential Dynamic Microscopy (DDM) and Convex Lens-induced Confinement (CLiC).

There has been much research done to investigate the dynamics of polymers in confinement, but direct determination of flexible polymer dynamics in a large range of confinement has been difficult to obtain. Davidson and Deen studied the diffusion of different water-soluble polymers in membranes and found that the diffusion is slowed as confinement increases.[11] Guo et al.[12] used Dynamic Light Scattering (DLS) to look at the diffusion of polystyrene in glass pores. Similar to Davidson and Deen, they found that the diffusion is slowed due to hydrodynamic changes near the surface and decreases monotonically with confinement. This is primarily due to the nonslip condition at the boundary. Sevick et al. have found that, for fluid−fluid interfaces, the nonslip condition no longer applies, which reduces the effect of hydrodynamic drag.[13] Bohrer et al.[14] further investigated the findings of Deen et al.[15] that examined the diffusion of two different polysaccharides, dextran and ficoll. All these hindered diffusion studies reached similar conclusions: that flexible polymers diffuse slower as the confinement increases, which is consistent with hydrodynamic theory.[11]

Recently, using CLiC and particle tracking, Berard et al.[16] found that DNA molecules diffuse slower with increasing confinement, which ranged from 100−150 nm. Leith et al.[17] used CLiC as well to determine how the conformational free energy of DNA molecules changes in confinement ranging from 100 to 1600 nm. Like Berard, Leith found that DNA molecules diffuse slower in strong confinement, and that the conformational free energy is much stronger than in the bulk. Because of these changes in conformational free energy, the DNA molecules were found to be more rod-like and extended in high confinement and more coil-like in the bulk. The Schwartz group has also used CLiC and particle tracking to study the dynamics of short DNA molecules in confinement ranging from 112.5−187.5 nm and polyelectrolyte surface diffusion.[18,19] They found that the DNA diffusion was hindered for shorter fragments as well. In the polyelectrolyte surface diffusion study, they found that chemically modifying the glass surface used in CLiC can affect the diffusion of poly-L-lysine in confinement. CLiC has been shown to be a versatile technique used to study confinement effects, but due to a lack of contrast, most of the research has focused on slower surface diffusion or diffusion of semiflexible polymers like DNA.

Received: January 9, 2023
Accepted: January 23, 2023
Published: January 27, 2023

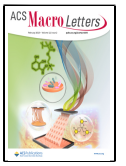

Light scattering ensemble-averaged techniques, such as DLS are well suited to investigate the dynamics of polymers in solution.[20,21] However, using DLS sacrifices real-space information and is generally limited in terms of sample preparation, whereas DDM can take real-space information and analyze it in the Fourier domain. By converting these real-space images into a Fourier domain, the real-space information will still be retained even in the Fourier-space analysis.[22] In this way, DDM is a powerful tool that can be used to determine diffusion in place of DLS. Previous studies conducted by Cerbino and Giavazzi have also confirmed that DDM can provide similar information to that of DLS and provides information at lower scattering wave vectors, q.[23,21,24−26] The main advantage of this technique is that optical resolution is not necessary, so diffusion studies of molecules not resolved in the microscope are possible, without the use of expensive camera setups. Because of this, DDM can be used to study the dynamics of flexible polymers and high concentrations of particles.[27,28] Notably, DDM can be used to analyze confocal, fluorescent microscopy, and other microscopy videos.[22] Recently, we have also shown that in a CLiC setup, DDM can be used to understand local viscosity changes due to surfaces and may be used as a powerful tool to investigate how different surface interactions change local dynamics.

In this Letter we report the dynamics of flexible polymers, such as dextran and sodium polyacrylate, near glass surfaces, and surfaces stabilized by a surfactant layer. To generate confinement, we have used CLiC techniques, with a total gap height range of 0.077−21.8 μm. We demonstrate that using the combination of DDM and CLiC makes studying flexible polymer dynamics in confinement feasible and will potentially lead to a better understanding of the behavior of model "foulants" near surfaces with different boundary conditions.

Dextran solutions were prepared by dissolving Sigma tetramethylrhodamine isothiocyanate (dextran; MW ∼ 500000 g/mol) and Invitrogen dextran, tetramethylrhodamine (70000 and 2000000 g/mol) in deionized water. The polymer was already fluorescently conjugated, with 3−6 dyes per 70000 g/mol, so no further action was necessary. The solutions were filtered through a 0.45 μm poly(ether sulfone) (PES) filter prior to imaging. While the 0.5−1 mg/mL experiments were repeated once, the 2 mg/mL data was repeated 3 times. Sodium polyacrylate (NaPA) solutions were prepared by dissolving 10 mg of Polymer Source poly(acrylic acid sodium salt) (M_n: 432000, M_w: 478000, PDI: 1.10) in 10 mL of DI water. It was then fluorescently tagged via a triazine coupling[29] using 125 μL of Alexa Fluor 488 dye and 30 mg of Aldrich 4-(4,6-dimethoxy-1,3,5-triazin-2-yl)-4-methylmorpholinium chloride (DMTMM). The DLS measurements were taken with the Brookhaven Instruments Corporation BI-200SM Goniometer. Before measurement, all solutions were filtered into clean vials with a 0.45 μm PES filter. Light scattering measurements were taken at angles θ = 50, 70, 90, 110, and 120°, using a laser with a wavelength ∼640 nm. The autocorrelation function was then fit with a cumulant fit with a relaxation rate Γ:

$$C(t) = A\ \exp\left(-2\Gamma\tau + K_2^2\tau^2 - \frac{K_3^3}{3}\tau^3\right) + B \tag{1}$$

here K_2 and K_3 are constants related to the dispersity and the skew of the distribution. Then the diffusion coefficient, D_0, was calculated from the slope of Γ versus q^2, assuming that the dynamics are Brownian:

$$D_0 = \frac{\Gamma}{q^2} \tag{2}$$

where q is the scattering vector, equal to $\frac{4\pi n}{\lambda}\sin(\theta/2)$, for which n is the index of refraction of the solvent (∼1.33) and λ is the laser wavelength.

To image and examine dextran diffusion in confinement, CLiC (Figure 1) was used in combination with DDM. A

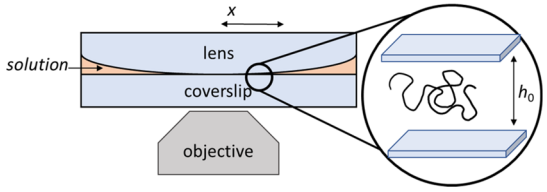

Figure 1. Convex lens-induced confinement setup.

TECHSPEC 25.4 mm diameter × 200 mm FL, uncoated ultrafast thin PCX convex lens (radius of curvature ∼ 91.80 mm) was secured on top of a 25 mm Electron Microscopy Sciences photoetched glass coverslip using an in-house 3D printed sample holder.[27] A 25 mm ruler was placed on top of the convex lens. The ruler, lens, and coverslip were cleaned with acetone and then rinsed with deionized water twice. The surfaces were then ozone etched using the Jelight UV-Ozone Model 24 for 15 min. This setup was secured on a 40 × 80 mm flat plate sample holder with four 15 mm height and 7 mm diameter posts. The Leica DMI 4000B microscope was used and connected to a Basler Ace camera, where a series of micrographs (480 × 480 pixels) were collected at 100−200 frames per second, depending on the molecular weight. The pixel size in these images is 0.064 μm. The exposure time was 5000−10000 μs, and an oil immersive 100× objective was used for all radial positions and heights. Two thousand micrographs were collected for each sample, and diffusion coefficients for four separate z locations within the channel, at the surface, 200 nm, 400 nm, and 1 μm, were averaged.

The heights within the channel were determined by loading a dye in a phosphate buffer saline solution in the CLiC setup. Three different Alexa Fluor 488 dye concentrations (0.01, 0.05, and 0.1 mg/mL) were imaged at the contact point at the same exposure time. The images were then azimuthally averaged to determine the height profile within the CLiC setup. The theoretical height was based off the curvature of the lens:[30]

$$h_0 = \frac{x^2}{2R_c} \tag{3}$$

where h_0 is the height within the channel, x is the radial distance from the contact point, and R_c is the lens radius of curvature.

DDM analyzes temporal intensity fluctuations, much like DLS. These intensity fluctuations are found by taking a time difference between all the images for different time intervals and is given by

$$I(\psi, t, \Delta t) = I(\psi, t + \Delta t) - I(\psi, t) \tag{4}$$

As shown in Figure S2, a Fourier transform is then done on these intensity fluctuations at different time delays and

https://doi.org/10.1021/acsmacrolett.3c00015
ACS Macro Lett. 2023, 12, 221−226

averaged out to produce the Intermediate Scattering Function (ISF):

$$\mathrm{ISF}(\boldsymbol{q}, \Delta t) = \langle |\Delta\hat{I}(\boldsymbol{q}, \Delta t)|^2 \rangle \quad (5)$$

Finally, the relaxation rates were obtained by fitting with

$$\mathrm{ISF}(q, \Delta t) = A(q)[1 - \exp(-\Gamma(q)\Delta t)] + B(q) \quad (6)$$

where $A(q)$ and $B(q)$ depend on the microscope's optical properties, and q is the wave-vector that corresponds to the inverse spatial position in the image, $q = 2\pi\sqrt{u_x^2 + u_y^2}$, where u_x and u_y are the coordinates of the image in the Fourier space.[27] Alternatively, if a single exponential fit is not able to capture the shape of the DDM function, a cumulant fit can be used:

$$\Delta(q, \tau) = A(q)\left[1 - \exp\left\{1 - \frac{\tau}{\tau_c(q)}\right\}\left(1 + \frac{\mu\tau^2}{2}\right)\right] + B(q) \quad (7)$$

where $\tau_c(q)$ is the wave-vector dependent relaxation time and $\mu\tau^2$ is the relative polydispersity.[31]

The DDM results are compared to DLS results in Figure 2 by plotting the averaged Γ versus q^2 data for 0.5, 1, and 2 mg/mL dextran in DI water at x = 2.0 mm, h_0 = 21.8 μm with the bulk DLS results. For our system, the DLS and DDM measurements are very similar (Table 1). While the data within each channel is very consistent, there is a spread of ~1.5 μm^2/s between independent trials, which makes the 0.5 and 1 mg/mL data within error of each other. We attribute any differences to the slightly different ways of determining the relaxation times, since a cumulant fit was used to analyze the DLS results. The NaPA data DLS and DDM data has been fit with a single exponential and are within error of each other. Therefore, DDM can be a comparable technique to DLS.

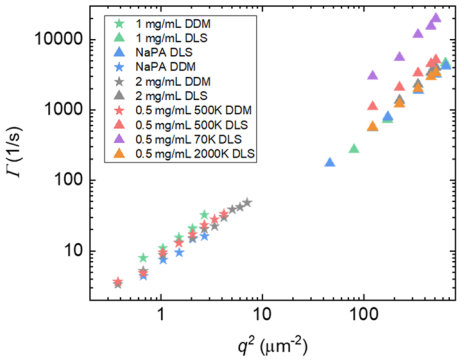

Figure 2. Comparison of DDM and DLS data for various dextran concentrations in the bulk.

Table 1. DDM and DLS Diffusion Coefficient and Hydrodynamic Radius Values for Various Dextran Concentrations

	D_0[a] (μm^2/s)			R_h (nm)	
(mg/mL)	DDM	DLS	PDI[b]	DDM	DLS
0.5 (500k)	8 ± 1	10 ± 1	0.5	26 ± 3	22 ± 2
1 (500k)	9 ± 0.8	8 ± 1	0.5	23 ± 2	26 ± 3
2 (500k)	7 ± 1.3	7 ± 1	0.5	31 ± 6	30 ± 4
0.5 (70k)		35 ± 1	0.6		6 ± 0.2
2 (70k)	47 ± 1			4.6 ± 0.1	
0.5 (2000k)		6 ± 1	0.5		35 ± 6
1 (NaPA)	6.5 ± 1	6 ± 1		34 ± 5	35 ± 6

[a]Measured at h_0 = 12−21.8 μm. [b]PDI = K_2/Γ^2.

From the Γ versus q^2 trends (Figure 2), the diffusion coefficient, D, was obtained. All the observed trends were linear, indicating there is Brownian motion within the channel.

In Figure 3b, all the diffusion coefficients are normalized by D_0 to give the mean relative diffusion coefficient, D/D_0. Here,

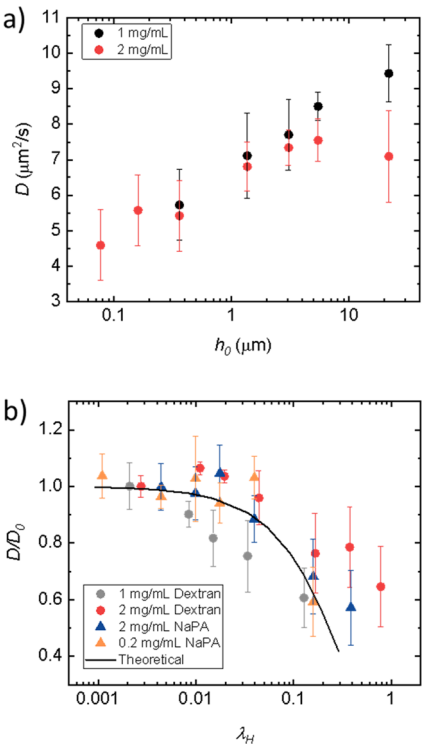

Figure 3. (a) Measured diffusion coefficient for 1 and 2 mg/mL as a function of total gap height h_0. (b) Normalized diffusion of 1 and 2 mg/mL dextran in deionized water as function of the confinement parameter, λ_H. Theoretical line is given by eq 9.

D_0 is the diffusion coefficient value at the gap height of 21.8 μm, which is considered to be the bulk dynamics regime (Table 1). D/D_0 is plotted against the confinement parameter λ_H, which is equal to $2R_h/h_0$. R_h is the hydrodynamic radius (~30 nm for dextran in the bulk) and h_0 is the confinement height ranging from 0.077−21.8 μm. R_h was calculated using the Stokes−Einstein equation:

$$D_0 = \frac{kT}{6\pi\eta R_h} \quad (8)$$

which relates D_0 to the hydrodynamic radius of the polymer.[11]

The experimental result matches the theoretical prediction of the diffusion of flexible, coiled, water-soluble polymers in confinement due to changes in hydrodynamics in a channel:[11]

$$\frac{D}{D_0} = \Phi K^{-1} \quad (9)$$

where Φ the partition coefficient, equal to $(1 - \lambda)^2$ for hard sphere interactions, and K^{-1} is the increased hydrodynamic drag on the macromolecule. According to Davidson and Deen:

$$K^{-1} = 1 - 2.848\lambda_H + 3.269\lambda_H^2 - 1.361\lambda_H^3 \quad (10)$$

https://doi.org/10.1021/acsmacrolett.3c00015
ACS Macro Lett. 2023, 12, 221−226

The model accounts for the hydrodynamic drag experienced by the macromolecules due to the confined space of the pore in the absence of interactions like electrostatics when flux is governed by diffusivity using the centerline approximation. The polynomial is an approximate solution from the calculated hydrodynamic model, tabulated in Davidson and Deen[32] accurate to within 2% for $\lambda \leq 0.87$.

Equation 9 is plotted in Figure 3b against the experimental results for 1 and 2 mg/mL dextran in deionized water. As λ_H tends to 0, D/D_0 for dextran for both 1 and 2 mg/mL concentrations is close to what is predicted theoretically. For the 1 mg/mL sample, diffusion is slower than expected, even in moderate confinement. For the 2 mg/mL, diffusion is higher than predicted. This may be attributed to the concentration dependence of D_0 and how the polymer partitions in the geometry. As shown in Figure 3a, the 1 and 2 mg/mL data are different in the "bulk", but quickly converge to the same value in confinement. It is known that the concentration in confinement is much lower than the bulk, and the two D values match for $h_0 < 5$ μm.[33] Similarly, the diffusion of the charged polymer NaPA follows eq 9. As the confinement increased, the signal became increasingly too weak to measure any diffusion for 0.2 mg/mL. Equation 9 also assumes a cylindrical pore, therefore, our experimental results may deviate from the theory provided. This can especially be important when considering that dextran is polydisperse and size separation is likely in confinement.

To study the effect of molecular weight, the diffusion of 70000, 500000, and 2000000 g/mol dextran solutions was determined (Figure 4). For $h_0 = 12.25$ μm, D scales as $\nu = 0.9$ with molecular weight, which is much larger than the DLS result of $\nu = 0.5$ for 0.5 mg/mL, consistent with the differences in fitting. At $\lambda_H \sim 0.02$, diffusion scales with molecular weight to the 0.44 power, which may indicate size partitioning in the channel, since the confinement is not strong enough to lead to conformational changes.[34] This value is expected for dextran and the larger $\nu = 0.9$ bulk value may be due to dispersity or aggregation in solution. In strong confinement to even intermediate confinement ($h_0 = 0.08-5.45$ μm), no diffusion was measured for the 2000000 g/mol dextran up to 5 mg/mL of total concentration. We assume that almost all high molecular weight dextran is adsorbed to the glass surface in that confinement region. Measured diffusion in the bulk ($h_0 = 12.25-21.8$ μm) is reported in the SI (Figure S7). Confocal images of the surfaces are in the SI (Figure S8).

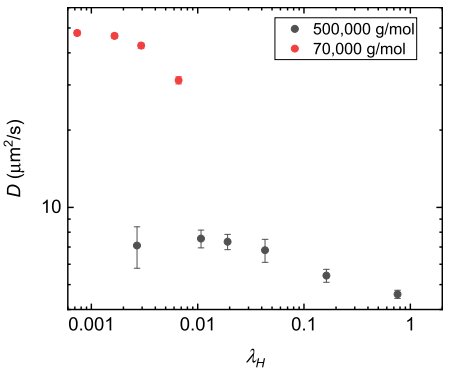

Figure 4. D vs λ_H for two molecular weight dextrans (70000 and 500000 g/mol).

The diffusion of dextran was further investigated on chemically modified surfaces. The surface was cleaned as described earlier and then treated with perfluorodecyltrichlorosilane via molecular vapor deposition, creating a hydrophobic monolayer on both the lens and coverslip. Triton X-100 was added to the dextran solutions below the critical micelle concentration to stabilize the hydrophobic surfaces in the CLiC setup. Interestingly, in strong confinement the diffusion on the modified surfaced varied drastically, compared to the unmodified surface, and fluctuated around a constant value, even as λ_H approached 1 (Figure 5). This indicates that either the surface treatment or the stabilizing surfactant layer suppressed changes in hydrodynamics near the glass surface. This has been observed for liquid−liquid interfaces, where diffusion is effected by the viscosity of both liquids and is an interesting finding that requires further study.[13,35,36] To completely understand how "softer" surfaces influence the surface-induced hydrodynamic drag, the DDM/CLiC setup may be used with other surface modifications, including lipid bilayers, polymer brushes, and gels.

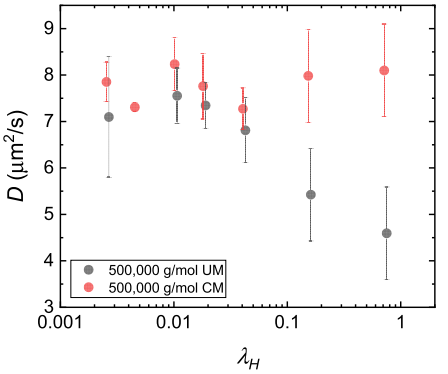

Figure 5. Measured diffusion vs λ_H for 2 mg/mL dextran (MW 500000 g/mol) on unmodified (UM) and chemically modified (CM) surfaces.

The behavior observed in these experiments demonstrates an important step in understanding the dynamics of flexible polymers in confinement, and the change in hydrodynamics as a function of surface treatment. In this letter, we demonstrate that DDM and CLiC can effectively be used to determine how flexible polymers diffuse near surfaces with different boundary conditions. The confinement range in this setup was from 0.077−21.8 μm. The diffusion of model polymers dextran and sodium polyacrylate slows down in high confinement, which is predicted by hydrodynamics. Near surfactant-stabilized hydrophobic surfaces, however, no change in dextran diffusion is observed. Ultimately, we believe that these results will be beneficial to future applications, including membrane separation, oil recovery, and much more. These findings also validate the use of CLiC and DDM in predicting the diffusion of these flexible polymers near complex surfaces.

■ ASSOCIATED CONTENT

Supporting Information

The Supporting Information is available free of charge at https://pubs.acs.org/doi/10.1021/acsmacrolett.3c00015.

Detailed description of all curve fitting for DDM and DLS (PDF)

https://doi.org/10.1021/acsmacrolett.3c00015
ACS Macro Lett. 2023, 12, 221−226

AUTHOR INFORMATION

Corresponding Author

Svetlana Morozova − *Department of Macromolecular Science and Engineering, Case Western Reserve University, Cleveland, Ohio 44106, United States;* orcid.org/0000-0002-1002-7413; Phone: 5088159802; Email: sam381@case.edu

Authors

Brittany K. Roopnarine − *Department of Macromolecular Science and Engineering, Case Western Reserve University, Cleveland, Ohio 44106, United States*

Spencer C. Schmidt − *Department of Macromolecular Science and Engineering, Case Western Reserve University, Cleveland, Ohio 44106, United States*

Kevin J. Maxwell − *Department of Macromolecular Science and Engineering, Case Western Reserve University, Cleveland, Ohio 44106, United States*

Complete contact information is available at: https://pubs.acs.org/10.1021/acsmacrolett.3c00015

Author Contributions

The manuscript was written through contributions of all authors.

Funding

This work was supported by ACS PRF# 61985-DNI7 and Case Western Reserve University startup funds.

Notes

The authors declare no competing financial interest.

ACKNOWLEDGMENTS

We would like to acknowledge Dr. Emmanuel Hitimana for helpful discussions.

REFERENCES

(1) Zhu, J.; Hou, J.; Zhang, Y.; Tian, M.; He, T.; Liu, J.; Chen, V. Polymeric Antimicrobial Membranes Enabled by Nanomaterials for Water Treatment. *J. Membr. Sci.* **2018**, *550*, 173−197.

(2) Lei, Q.; Zhang, M.; Shen, L.; Li, R.; Liao, B. Q.; Lin, H. A Novel Insight into Membrane Fouling Mechanism Regarding Gel Layer Filtration: Flory-Huggins Based Filtration Mechanism. *Sci. Rep.* **2016**, *6*, 33343.

(3) Li, Q.; Elimelech, M. Organic Fouling and Chemical Cleaning of Nanofiltration Membranes: Measurements and Mechanisms. *Environ. Sci. Technol.* **2004**, *38* (17), 4683−4693.

(4) Lin, N. H.; Kim, M. M.; Lewis, G. T.; Cohen, Y. Polymer Surface Nano-Structuring of Reverse Osmosis Membranes for Fouling Resistance and Improved Flux Performance. *J. Mater. Chem.* **2010**, *20* (22), 4642−4652.

(5) Liu, G.; Yu, S.; Yang, H.; Hu, J.; Zhang, Y.; He, B.; Li, L.; Liu, Z. Molecular Mechanisms of Ultrafiltration Membrane Fouling in Polymer-Flooding Wastewater Treatment: Role of Ions in Polymeric Fouling. *Environ. Sci. Technol.* **2016**, *50* (3), 1393−1402.

(6) Li, X.; Xu, Z.; Yin, H.; Feng, Y.; Quan, H. Comparative Studies on Enhanced Oil Recovery: Thermoviscosifying Polymer Versus Polyacrylamide. *Energy Fuels* **2017**, *31* (3), 2479−2487.

(7) Roda, A.; Matias, A. A.; Paiva, A.; Duarte, A. R. C. Polymer Science and Engineering Using Deep Eutectic Solvents. *Polymers* **2019**, *11*, 912.

(8) Zhang, S.; Ye, L.; Zhang, H.; Hou, J. Green-Solvent-Processable Organic Solar Cells. *Mater. Today* **2016**, *19* (9), 533−543.

(9) Susanto, H.; Franzka, S.; Ulbricht, M. Dextran Fouling of Polyethersulfone Ultrafiltration Membranes-Causes, Extent and Consequences. *J. Membr. Sci.* **2007**, *296* (1−2), 147−155.

(10) Susanto, H.; Ulbricht, M. Influence of Ultrafiltration Membrane Characteristics on Adsorptive Fouling with Dextrans. *J. Membr. Sci.* **2005**, *266* (1−2), 132−142.

(11) Davidson, M. G.; Deen, W. M. Hindered Diffusion of Water-Soluble Macromolecules in Membranes. *Macromolecules* **1988**, *21* (12), 3474−3481.

(12) Guo, Y.; Langley, K. H.; Karasz, F. E. Hindered Diffusion of Polystyrene in Controlled Pore Glasses. *Macromolecules* **1990**, *23*, 2022−2027.

(13) Wang, G. M.; Prabhakar, R.; Sevick, E. M. Hydrodynamic Mobility of an Optically Trapped Colloidal Particle near Fluid-Fluid Interfaces. *Phys. Rev. Lett.* **2009**, *103* (24), 248303.

(14) Bohrer, M. P.; Patterson, G. D.; Carroll, P. J. Hindered Diffusion of Dextran and Ficoll in Microporous Membranes. *Macromolecules* **1984**, *17* (6), 1170−1173.

(15) Deen, W. M.; Bohrer, M. P.; Epstein, N. B. Effects of Molecular Size and Configuration on Diffusion in Microporous Membranes. *AIChE J.* **1981**, *27* (6), 952−959.

(16) Berard, D.; McFaul, C. M. J.; Leith, J. S.; Arsenault, A. K. J.; Michaud, F.; Leslie, S. R. Precision Platform for Convex Lens-Induced Confinement Microscopy. *Rev. Sci. Instrum.* **2013**, *84* (10), 103704.

(17) Leith, J. S.; Kamanzi, A.; Sean, D.; Berard, D.; Guthrie, A. C.; McFaul, C. M. J.; Slater, G. W.; De Haan, H. W.; Leslie, S. R. Free Energy of a Polymer in Slit-like Confinement from the Odijk Regime to the Bulk. *Macromolecules* **2016**, *49* (23), 9266−9271.

(18) Morrin, G. T.; Kienle, D. F.; Schwartz, D. K. Diffusion of Short Semiflexible DNA Polymer Chains in Strong and Moderate Confinement. *ACS Macro Lett.* **2021**, *10* (10), 1191−1195.

(19) Morrin, G. T.; Kienle, D. F.; Weltz, J. S.; Traeger, J. C.; Schwartz, D. K. Polyelectrolyte Surface Diffusion in a Nanoslit Geometry. *Macromolecules* **2020**, *53* (10), 4110−4120.

(20) Borsali, R., Percora, R., Eds. *Soft Matter Characterization*; Springer, 2008. DOI: 10.1007/978-1-4020-4465-6.

(21) Lu, P. J.; Giavazzi, F.; Angelini, T. E.; Zaccarelli, E.; Jargstorff, F.; Schofield, A. B.; Wilking, J. N.; Romanowsky, M. B.; Weitz, D. A.; Cerbino, R. Characterizing Concentrated, Multiply Scattering, and Actively Driven Fluorescent Systems with Confocal Differential Dynamic Microscopy. *Phys. Rev. Lett.* **2012**, *108* (21), 1−5.

(22) Cerbino, R.; Giavazzi, F.; Helgeson, M. E. Differential Dynamic Microscopy for the Characterization of Polymer Systems. *J. Polym. Sci.* **2022**, *60*, 1079−1089.

(23) Giavazzi, F.; Cerbino, R. Digital Fourier Microscopy for Soft Matter Dynamics. *J. Opt. (United Kingdom)* **2014**, *16* (8), 083001.

(24) Giavazzi, F.; Brogioli, D.; Trappe, V.; Bellini, T.; Cerbino, R. Scattering Information Obtained by Optical Microscopy: Differential Dynamic Microscopy and Beyond. *Phys. Rev. E* **2009**, *80* (3), 31403.

(25) Cerbino, R.; Trappe, V. Differential Dynamic Microscopy: Probing Wave Vector Dependent Dynamics with a Microscope. *Phys. Rev. Lett.* **2008**, *100* (18), 1−4.

(26) Wilson, L. G.; Martinez, V. A.; Schwarz-Linek, J.; Tailleur, J.; Bryant, G.; Pusey, P. N.; Poon, W. C. K. Differential Dynamic Microscopy of Bacterial Motility. *Phys. Rev. Lett.* **2011**, *106* (1), 18101.

(27) Hitimana, E.; Roopnarine, B. K.; Morozova, S. Diffusive Dynamics of Charged Nanoparticles in Convex Lens-Induced Confinement. *Soft Matter* **2022**, *18* (4), 832−840.

(28) Bayles, A. V.; Squires, T. M.; Helgeson, M. E. Probe Microrheology without Particle Tracking by Differential Dynamic Microscopy. *Rheol. Acta* **2017**, *56* (11), 863−869.

(29) Thompson, K.; Michielsen, S. Novel Synthesis of N-Substituted Polyacrylamides: Derivatization of Poly(Acrylic Acid) with Amines Using a Triazine-Based Condensing Reagent. *J. Polym. Sci. Part A Polym. Chem.* **2006**, *44* (1), 126−136.

(30) Morrin, G. T.; Kienle, D. F.; Schwartz, D. K. Standalone Interferometry-Based Calibration of Convex Lens-Induced Confinement Microscopy with Nanoscale Accuracy. *Analyst* **2019**, *144* (8), 2628−2634.

(31) Safari, M. S.; Vorontsova, M. A.; Poling-Skutvik, R.; Vekilov, P. G.; Conrad, J. C. Differential Dynamic Microscopy of Weakly

Scattering and Polydisperse Protein-Rich Clusters. *Phys. Rev. E* **2015**, *92* (4), 42712.
(32) G. Davidson, M.; M. Deen, W. Hydrodynamic Theory for the Hindered Transport of Flexible Macromolecules in Porous Membranes. *J. Membr. Sci.* **1988**, *35* (2), 167−192.
(33) Day, J. C.; Alince, B.; Robertson, A. A. Interaction of Polymers in Solution with Porous Solids. I. Penetration of Porous Glass by Dextran. *Can. J. Chem.* **1978**, *56* (23), 2951−2958.
(34) Hiemenz, P. C.; Lodge, T. P.*Polymer Chemistry*, 2nd ed.; Taylor and Francis, 2007. DOI: 10.1201/9781420018271.
(35) Wang, G. M.; Prabhakar, R.; Gao, Y. X.; Sevick, E. M. Micro-Rheology near Fluid Interfaces. *J. Opt.* **2011**, *13* (4), 044009.
(36) Daddi-Moussa-Ider, A.; Gekle, S. Hydrodynamic Interaction between Particles near Elastic Interfaces. *J. Chem. Phys.* **2016**, *145* (1), 014905.

https://doi.org/10.1021/acsmacrolett.3c00015
ACS Macro Lett. 2023, 12, 221−226